Phasons, amplitude modes, and spin waves in the amplitude-modulated magnetic phase of $PrNi_2Si_2$

J. A. Blanco,[1] B. Fåk,[2] J. Jensen,[3] M. Rotter,[4] A. Hiess,[5,*] D. Schmitt,[6] and P. Lejay[7]

[1]*Departamento de Física, Universidad de Oviedo, E-33007 Oviedo, Spain*
[2]*SPSMS, UMR-E CEA/UJF-Grenoble-1, INAC, 38054 Grenoble Cedex 9, France*
[3]*Niels Bohr Institute, Universitetsparken 5, DK-2100 Copenhagen, Denmark*
[4]*Max-Planck Institute for Chemical Physics of Solids, 01187 Dresden, Germany*
[5]*Institut Laue Langevin, 156X, 38042 Grenoble cedex 9, France*
[6]*ISTerre, CNRS, Université de Grenoble 1, F-38041 Grenoble, France*
[7]*Institut Néel, CNRS, BP 166, 38042 Grenoble Cedex 9, France*

(Received 18 December 2012; revised manuscript received 18 January 2013; published 20 March 2013)

The magnetic excitations in the low-temperature amplitude-modulated magnetic structure of $PrNi_2Si_2$ have been investigated by inelastic neutron scattering. The dispersions and intensities of both longitudinal and transverse excitations are measured along the high-symmetry directions. The modulated magnitude of the ordered moments implies that the longitudinally polarized magnetic excitations are more intense and dispersive than the usual transverse spin waves. Several well-defined longitudinal amplitude modes are observed to coexist with the longitudinal phason mode. The experimental results are in good overall agreement with predictions from the random-phase approximation, using parameters already established from the macroscopic properties and the paramagnetic excitations. At low energies in the neighborhood of the magnetic zone center, the magnetic phason appears to hybridize with an unidentified dispersionless mode.

DOI: 10.1103/PhysRevB.87.104411 PACS number(s): 75.25.−j, 75.10.Dg, 75.50.Ee, 75.30.Ds

I. INTRODUCTION

In nature there is a large variety of systems whose physical properties depend crucially on the interplay of two, or more, different length scales. When one scale is set by a lattice unit cell dimension, the second scale can usefully be regarded as imposing a modulation which, in most of the cases, is incommensurate with the lattice.[1–5] In magnetic systems, the modulation may arise from geometrical frustration related to the topology of the crystal lattice or from competing exchange interactions, which both forbid the simultaneous minimization of the interaction energies acting at a given site.[6,7]

Spatially modulated systems are being intensively studied, where the periodic phase is a lattice distortion, a charge-density wave, or an ordered magnetic structure.[8–12] Many rare-earth intermetallic compounds exhibit amplitude-modulated (AM) magnetic ordering, where the magnetic moment changes amplitude from one site to another. This is a consequence of strong easy-axis crystal-field (CF) anisotropy and frustration from competing interactions due to the oscillatory and long-range character of the indirect Ruderman-Kittel-Kasuya-Yosida (RKKY) exchange interaction mediated by the conduction-band electrons.[13–16] These magnetic structures are often observed only in the vicinity of the ordering temperature. Expanding the free energy in even powers of the order parameter,[17] the fourth- and higher-order terms that come into play at lower temperatures destabilize the AM structures and favor equal-moment ordered phases in the limit of zero temperature. A noticeable exception are CF singlet ground-state systems,[17] where the exchange interaction induces a magnetic moment by mixing the singlet state with the excited states. The magnitude of the induced moment in the ground state depends strongly on the strength of the exchange field, hence allowing a variation of the length of the ordered moments even in the zero-temperature limit. AM magnetic structures are characterized by a propagation vector $\boldsymbol{\tau}$, which is in general incommensurate with the crystal lattice, or which in the commensurate case corresponds to a magnetic unit cell consisting of several crystallographic unit cells. Due to the modification of the translational symmetry, the magnetic excitations display properties different from the spin waves in ferromagnetic or simple antiferromagnetic structures. Excitations in incommensurate magnetic structures are also thought to be of great importance for unconventional superconductivity.[18,19] A particularity of low-temperature AM structures is that they may support the presence of well-defined longitudinal excitations, which derive from a modulation of the amplitudes of the moments. In most "equal-moment"systems the moments saturate at low temperatures, in which case the longitudinal excitations are quenched, allowing only the presence of transversely polarized spin waves. In this work, longitudinal and transverse excitations refer to the direction of the magnetic fluctuations with respect to the ordered moment and not with respect to the direction of the propagation vector.

Well-known examples of AM magnetic structures are Tm and Er hcp metals,[20] where the ordered magnetic moments and the ordering wave vectors are parallel to the hexagonal c axis. In the case of Er, the AM phase is stable only between T_N and $0.6\,T_N$. In Tm, the magnetic structure stays longitudinally modulated for all temperatures below T_N, but the ordered moments are completely squared up in a seven-layered commensurate equal-moment structure in the zero-temperature limit. This means that transverse spin waves are the dominating magnetic excitations at low temperatures in these two systems.[22,23] Another example is Pr metal, a singlet ground-state system, where a longitudinally polarized ordered phase is induced by the application of uniaxial pressure, and in this phase well-defined longitudinal magnetic excitations have been observed far below the Néel temperature.[24]

$PrNi_2Si_2$ is of particular interest in this context,[25–27] as it represents one of the few examples exhibiting an AM

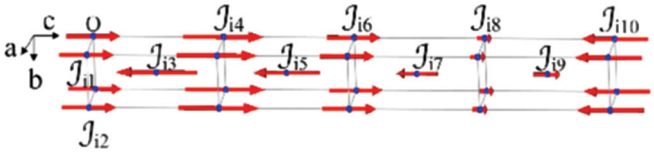

FIG. 1. (Color online) Schematic representation of the low-temperature amplitude-modulated magnetic structure of $PrNi_2Si_2$ showing the Pr^{3+} ions and their magnetic moments. The exchange constants $\mathcal{J}_{ij}$ defined in Table I between ion i at the origin O and the positions j are indicated. The magnetic moments are obtained by self-consistently solving the Hamiltonian Eq. (1).

magnetic structure that is stable down to zero temperature. It crystallizes in a body-centered tetragonal structure with space group $I4/mmm$ (No. 139) and lattice parameters $a = 4.047$ and $c = 9.621$ Å.[27,28] The ordered magnetic moments are confined to be along the c axis (see Fig. 1) by the single-ion anisotropy, evidenced by the magnetic susceptibility ratio of $\chi_c/\chi_a \approx 4.5$ above $T_N = 20$ K. The magnetic structure at low temperature (4 K) is well described by a single propagation vector $\boldsymbol{\tau} = (0,0,0.87)$ and an ordered moment of 2.35 μ_B.[27] At even lower temperatures the observation of a third harmonic at $3\boldsymbol{\tau}$ reflects a weak tendency to "squaring up" of the AM moment, but the observed moment ratio of $M_{3\boldsymbol{\tau}}/M_{\boldsymbol{\tau}} \sim 1/7$ is far from the limit of complete squaring, $M_{3\boldsymbol{\tau}}/M_{\boldsymbol{\tau}} = 1/3$.[17,27] Since studies of the magnetic excitations in $PrNi_2Si_2$ below T_N are scarce,[29–31] we have performed new inelastic neutron-scattering measurements of the dispersive low-energy excitations. The data obtained are analyzed using the random-phase approximation (RPA).

The RPA theory is outlined in Sec. II. Section III describes the experimental setup. The experimental results are presented and compared with the predictions from the RPA model in Sec. IV. In Sec. V we discuss the low-energy dynamics that is not fully captured by the RPA model. Section VI concludes the paper.

II. RPA MODEL

A. Crystal field and exchange interactions

In $PrNi_2Si_2$, the crystalline electric field (point group D_{4h}, quantization axis c) splits the ninefold degenerate Hund's rule ground-state multiplet $^3H_4$ of the Pr^{3+} ions with total angular momentum $J = 4$ into five singlets and two doublets.[32] The next multiplet state is ∼300 meV higher in energy.[33] The Hamiltonian can be written

$$\mathcal{H} = \sum_i \sum_{\ell,m} B_\ell^m O_\ell^m(i) - \frac{1}{2}\sum_{ij} \mathcal{J}_{ij}\mathbf{J_i}\cdot\mathbf{J_j}, \qquad (1)$$

where the first term contains the crystal-field single-ion contributions involving only $m = 0$ for $\ell = 2$ and $m = 0,4$ for $\ell = 4,6$, and where O_l^m and B_l^m are the Stevens operators and CF parameters, respectively.[34] The second term in Eq. (1) is the isotropic RKKY exchange interaction, where $\mathcal{J}_{ij}$ are the exchange coupling parameters and $\mathbf{J}_i$ the total angular momentum on site i. The magnetic dipole-dipole coupling is neglected in view of the small moment magnitude.

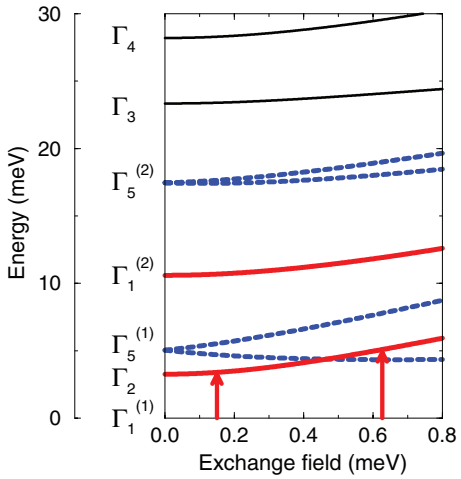

FIG. 2. (Color online) Mean-field excitation energies for the Pr^{3+} ions as functions of an exchange field ($g\mu_B H$) along the z axis, calculated with the use of the CF parameters given in Table I. The classification of the levels is the one applying at zero exchange field. The two singlets shown by the (red) solid lines are only coupled to the ground state by J_z, whereas the matrix elements of J_x and J_y between the ground state and the excited states are only nonzero for the four Γ_5 states shown by the (blue) dashed lines. The J_z matrix element between the ground state and $\Gamma_1^{(2)}$ vanishes at zero field and is a factor of 5 smaller than the other J_z matrix element at the maximum exchange field. In the AM phase at $T = 1.6$ K, the numerical value of the exchange field varies between the two limits denoted by the (red) arrows. The lower limit only applies for the commensurate structure assumed in the present analysis.

A joint analysis of specific heat, magnetization, magnetic susceptibility, and inelastic neutron-scattering measurements above T_N suggests a singlet CF ground state $\Gamma_1^{(1)}$, which is responsible for the tetragonal easy-axis single-ion anisotropy.[15,16] The first excited state is a singlet Γ_2 at an energy of 3.3 meV and the second a doublet $\Gamma_5^{(1)}$ at 5.0 meV. The remaining $J = 4$ levels lie at higher energies (see Fig. 2). They are retained in the model calculations but are of no concern for the low-energy magnetic excitations studied in this work or the ground-state properties.[16]

The exchange couplings responsible for the incommensurate AM magnetic ordering below T_N were determined from the dispersion of the low-energy longitudinal mode in the *paramagnetic* phase of $PrNi_2Si_2$.[25] The values are reproduced in Table I.

B. Mean-field/random-phase approximation

To calculate the magnetic excitations in the ordered phase within the RPA, we treat Eq. (1) in the mean-field (MF) approximation.[22,23] The incommensurate propagation vector is approximated by an effective commensurate one, $\boldsymbol{\tau}_{\rm eff} \equiv (0,0,7/8) \cong (0,0,0.87)$. This means that the magnetic unit cell is assumed to be eight times as long as the body-centered tetragonal unit cell, corresponding to a period of 16 atomic Pr layers along the c axis.

TABLE I. Isotropic bilinear exchange and crystal-field parameters derived from the paramagnetic properties of $PrNi_2Si_2$. The exchange parameters represent the couplings between neighboring ions whose relative positions are $\mathbf{r} = (n_1a, n_2a, n_3c)$, and the labels are defined in Fig. 1.

	$n_1\,n_2\,n_3$	100	110	$\frac{1}{2}\frac{1}{2}\frac{1}{2}$	001	$\frac{1}{2}\frac{1}{2}\frac{3}{2}$	002	$\frac{1}{2}\frac{1}{2}\frac{5}{2}$	003	$\frac{1}{2}\frac{1}{2}\frac{7}{2}$	004
Exchange parameters[a]	$\mathcal{J}_{ij}$	$\mathcal{J}_{i1}$	$\mathcal{J}_{i2}$	$\mathcal{J}_{i3}$	$\mathcal{J}_{i4}$	$\mathcal{J}_{i5}$	$\mathcal{J}_{i6}$	$\mathcal{J}_{i7}$	$\mathcal{J}_{i8}$	$\mathcal{J}_{i9}$	$\mathcal{J}_{i10}$
Number of neighbors		4	4	8	2	8	2	8	2	8	2
	[μeV]	5.95	7.84	−15.6	12.2	−0.34	−2.07	1.55	−0.43	1.12	−4.83
			B_2^0		B_4^0		B_4^4		B_6^0		B_6^4
Crystal-field parameters[b]	[μeV]		−311		−2.39		−20.2		0.34		−0.48

[a]Taken from Ref. 25.
[b]Taken from Ref. 16.

The neutron-scattering intensity is given by

$$S(\mathbf{Q},\omega) = -\frac{1}{\pi}\frac{1}{1-\exp(-\hbar\omega/k_BT)}|f(\mathbf{Q})|^2 \times \sum_{\alpha\beta}\left(\delta_{\alpha\beta}-\frac{Q_\alpha Q_\beta}{|\mathbf{Q}|^2}\right)\mathrm{Im}\{G^{\alpha\beta}_{n=0}(\mathbf{Q},\omega)\}, \quad (2)$$

where Q_α are the Cartesian components of the neutron-scattering vector $\mathbf{Q}$ and $f(\mathbf{Q})$ the magnetic form factor of the Pr^{3+} ions. Since the magnetic unit cell has 16 nonequivalent sites, $n = 0,\ldots,15$, the corresponding Fourier-transformed two-site Green's functions are coupled within the RPA theory through[21,23]

$$\overline{\overline{G}}_n(\mathbf{q},\omega) = \overline{\overline{g}}_n(\omega) - \sum_{s=0}^{15}\overline{\overline{g}}_{n-s}(\omega)\overline{\overline{\mathcal{J}}}(\mathbf{q}+s\,\boldsymbol{\tau})\overline{\overline{G}}_s(\mathbf{q},\omega), \quad (3)$$

where $\mathbf{q}$ is the wave vector and $\overline{\overline{g}}_n(\omega)$ the nth Fourier component of the single-site dynamical magnetic susceptibility with negative sign calculated from the mean-field levels of the magnetic system shown in Fig. 2. The 16 equations of 3×3 matrices in Eq. (3) may be solved numerically after the introduction of a small imaginary energy width ϵ. The positions of the poles or the excitation energies have also been determined directly using the dynamical matrix-diagonalization method implemented in the McPhase software package.[35]

The modulation of the magnetic moments in the AM structure introduces a coupling between the excitations at wave vectors $\mathbf{q}$ and $\mathbf{q}\pm n\boldsymbol{\tau}$, according to Eq. (3). The longitudinal cc (or zz) component of the single-site Green's function $\overline{\overline{g}}_n(\omega)$ determined by the J_z matrix elements in Fig. 2 is decoupled from the transverse (J_x, J_y) part. If the exchange interaction is assumed to be isotropic, the same remains true for all wave vectors in the final two-site Green's function.

We first discuss the longitudinal excitations. In the paramagnetic phase, the low-energy cooperative excitations with longitudinal (cc) polarization correspond to J_z transitions between the $\Gamma_1^{(1)}$ and the Γ_2 state at zero exchange field. Below T_N, the longitudinal magnetic excitations derive from the same transition at nonzero exchange fields. The cc component $g_n^{cc}(\omega)$ is invariant with respect to reversal of the ordered moment at site n. This means that if the commensurate period comprises an even number of layers (16 in the present case), the effective commensurate period becomes half the actual one, i.e., the width of the magnetic Brillouin zone is effectively doubled along the c axis for the longitudinal part of the excitation spectrum (ΔL is 0.25 rather than 0.125). The cc components in Eq. (3) involve only the even harmonics ($n = 0,2,\ldots,14$), and the strongest off-diagonal interaction occurs between the longitudinal modes at $\boldsymbol{\tau}+\mathbf{q}$ and $\boldsymbol{\tau}-\mathbf{q}$. Close to $\boldsymbol{\tau}$ this interaction leads to two modes: a phason mode and an amplitude mode. The phason mode is a gapless Goldstone mode of the magnetic system and can be pictured as 90° out-of-phase modulation of the lengths of the magnetic moments in the AM ordered structure. Close to a magnetic Bragg point, the phason mode has a linear dispersion starting out with zero energy from the magnetic Bragg point. However, the Goldstone mode picture is an approximation. In the "truly"incommensurate case the phason mode becomes diffusive close to the magnetic Bragg point (see, for instance, the discussion in Ref. 23) and in the commensurate case, where no continuous magnetic symmetry is broken, it becomes a pseudo-Goldstone mode with a nonzero energy gap at the magnetic Bragg point. In the present system, the RPA theory predicts the gap to be very small, about 0.1 meV when $\boldsymbol{\tau} \equiv (0,0,7/8)$, indicating that, in practice, it is not important whether $\boldsymbol{\tau}$ is commensurate or not. The amplitude mode is a less intense gapped excitation, associated with an in-phase magnetic-moment modulation. The relatively large amplitude of the first harmonic in $PrNi_2Si_2$, which is 58% of the saturated squared-up value at 1.6 K, implies that one would expect strong intensity of the amplitude modes in $PrNi_2Si_2$.

The transverse spin waves in the AM phase derive from the $J_\perp$ transitions between the $\Gamma_1^{(1)}$ ground-state singlet and the $\Gamma_5^{(1)}$ doublet in the paramagnetic state. The magnetic Brillouin zone is shorter by a factor of 2 and, in principle, the number of branches is doubled. Furthermore, since the $\Gamma_5^{(1)}$ doublet is split in two nondegenerate levels due to the exchange field, see Fig. 2, the number of branches is 2×16. The transverse spin waves are only weakly dispersive and closely spaced, and would be difficult to separate experimentally.

Figure 3 shows the calculated correlation functions predicted by the RPA theory using the model defined by the parameters in Table I carried out with a narrow resolution. The effective magnetic Brillouin zone for the longitudinal excitations along $(1,1,L)$ in Fig. 3(a) has the length $\Delta L = 0.25$ and each zone contains one phason mode (the lowest branch) plus seven amplitude modes (the one lying between 3.5 and 4 meV consists of two nearly degenerate branches). The

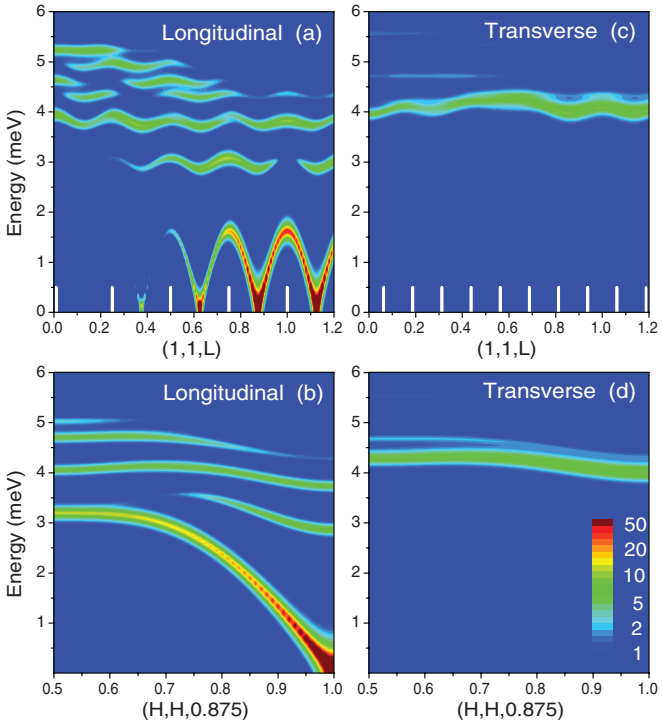

FIG. 3. (Color online) RPA correlation functions on a logarithmic scale at $T = 1.6$ K predicted by the model defined in Table I. (a), (b) Longitudinal excitation spectrum (cc components) along the $(1,1,L)$ and $(H,H,0.875)$ directions, respectively. (c), (d) Corresponding transverse spin waves (aa components). The magnetic zone boundaries along $(1,1,L)$ in (a), (c) are indicated by white vertical lines.

different modes are separated by energy gaps at the zone boundaries at L equal to integer multiples of 0.25. The energies are the same within each zone, but the weights of the different branches depend on the absolute positions of the zones roughly so that the closer a branch is to the corresponding single branch of paramagnetic cc excitations the more intense it is. The calculated dispersion of the transverse spin waves is shown in Figs. 3(c) and 3(d).

III. EXPERIMENTAL DETAILS

Inelastic neutron-scattering measurements were performed in the $(H\,H\,L)$ plane (see Fig. 4) on the cold-neutron triple-axis spectrometer IN14 at the Institut Laue-Langevin (Grenoble) with vertically focusing PG(002) monochromator and analyzer, a 40' collimator before the sample, and a liquid-nitrogen Be filter after the sample to reduce background and higher-order contamination. The final wave vector k_f was kept fixed, and three different configurations were used resulting in an energy resolution ΔE of the incoherent elastic scattering as follows: $k_f = 1.50$ Å^{-1}, horizontal focusing, $\Delta E = 0.210$ meV; $k_f = 1.30$ Å^{-1}, horizontal focusing, $\Delta E = 0.125$ meV; $k_f = 1.30$ Å^{-1}, flat analyzer, $\Delta E = 0.080$ meV. The data were normalized to higher-order corrected monitor counts. We used the same 1 cm^3 Czochralski-grown $PrNi_2Si_2$ single crystal as in Ref. 25. Most measurements were performed at a temperature of 1.6 K, with a few complementary scans taken between 1.6 and 20 K. In this work, we focus on the

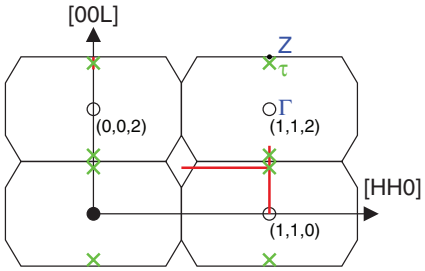

FIG. 4. (Color online) $(H\,H\,L)$ plane of the reciprocal lattice of $PrNi_2Si_2$. Thin (black) lines show the Brillouin zones, (black) circles nuclear zone centers, and (green) crosses positions of the magnetic Bragg peaks corresponding to the propagation vector $\boldsymbol{\tau} = (0,0,0.87)$. Special positions are labeled with (blue) letters, while (red) thick lines show the principal high-symmetry scan directions.

low-energy excitations, below 6 meV, knowing that there are excitations also at higher energies, as indicated in the level scheme of Fig. 2. The polarization of the magnetic excitations was determined from their **Q** dependence, using the fact that neutrons observe only moments (or moment fluctuations) that are perpendicular to the wave-vector transfer **Q**.

IV. RESULTS

Energy scans in the magnetically ordered phase of $PrNi_2Si_2$ at $T = 1.6$ K along the two main symmetry directions $[00\ell]$ and $[hh0]$ starting from the magnetic zone center at $\mathbf{Q} = (1,1,0.88)$ are shown in an overview in Figs. 5(a)–5(c). For comparison we also show [see Figs. 5(d)–5(f)] the corresponding RPA results predicted by the parameters derived previously from the paramagnetic properties and given in Table I, i.e., the neutron-scattering cross sections obtained from the longitudinal and transverse correlation functions in Fig. 3 when folded with a Gaussian corresponding to the experimental resolution.

The polarization of the excitations was determined from energy scans in the $[0,0,\ell]$ direction, as shown in Fig. 6. At $\mathbf{Q} = (0,0,L)$ [Figs. 6(a)–6(c)], only transverse excitations can be observed by neutron scattering, while at $\mathbf{Q} = (1,1,L)$ [Figs. 6(d)–6(f)] both transverse and longitudinal excitations are probed. Clearly, the transverse excitations are confined to a narrow range of energy centered at about 4–5 meV. The RPA model calculations indicate that this clear separation should be true also at wave vectors which have a component perpendicular to the c axis (see Fig. 3), and this was checked experimentally by comparing scans at $(0.15,0.15,L + 0.88)$ and $(0.4,0.4,L + 0.88)$ for $L = 0$ and $L = 2$. We conclude that all excitations below approximately 4 meV are due exclusively to longitudinal excitations, whereas, in general, the intensities observed above 4 meV derive from a mixture of scattering from both longitudinal and transverse excitations. The comparison between experiments and theory along $(H,H,0.88)$ given by Figs. 5(a) and 5(c) at energies below 4 meV allows a clear identification of the phason mode evolving with a linear dispersion from the magnetic Bragg peak at (1,1,0.87) and the principal amplitude mode starting out from the magnetic Bragg point with an energy of about 3 meV. Along $(1,1,L)$ the theory predicts an energy gap separation between the low-energy phason mode below 2 meV and the amplitude

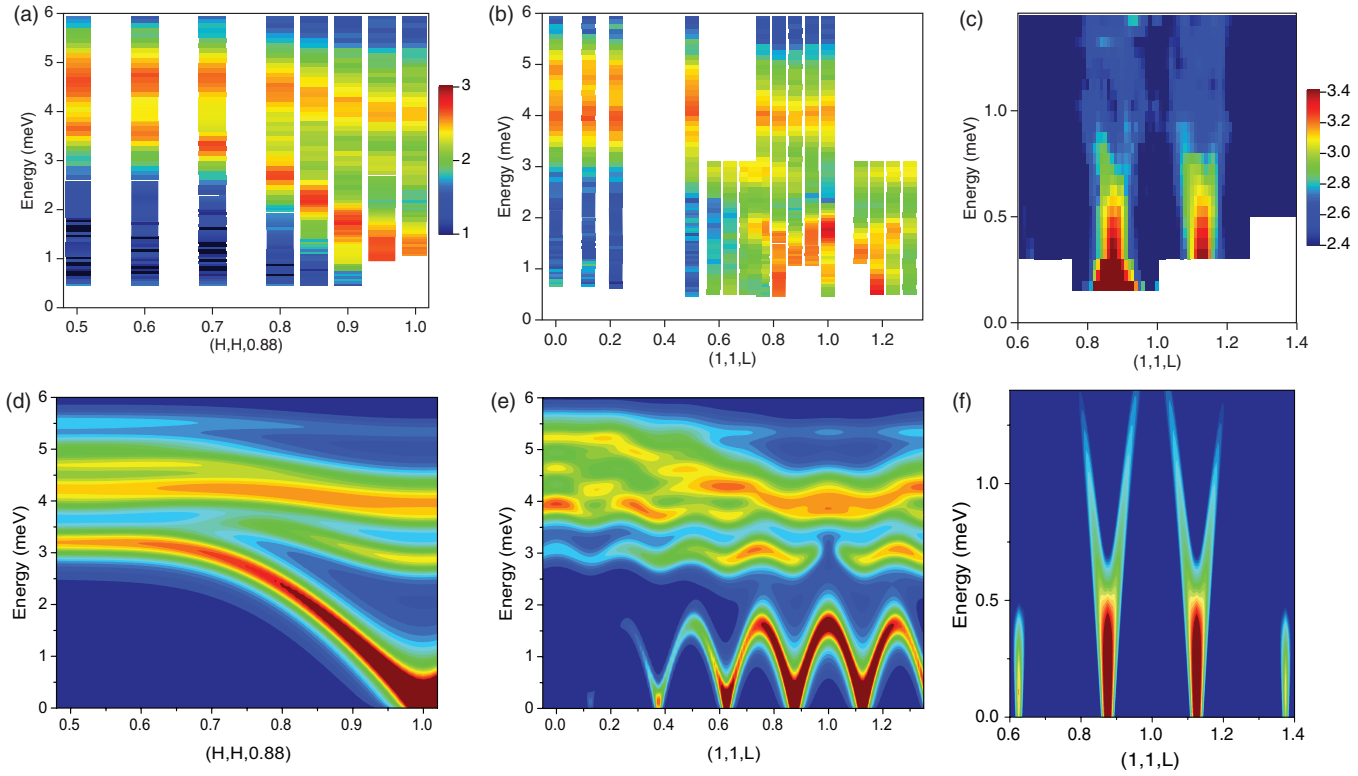

FIG. 5. (Color online) (a)–(c) Neutron scattering intensity of the magnetic excitations in $PrNi_2Si_2$ at $T = 1.6$ K on a logarithmic scale as a function of wave vector and energy. (a) Along $(H,H,0.88)$ and (b) along $(1,1,L)$ using $k_f = 1.50$ Å^{-1}. (c) Along $(1,1,L)$ close to the magnetic zone center with higher resolution using $k_f = 1.30$ Å^{-1} and flat analyzer. (d)–(f) Corresponding RPA results obtained from the model presented in Table I.

mode at about 3 meV, which is clearly resolved experimentally as shown in Fig. 5(b). Several higher-order longitudinal amplitude modes are resolved in the experiment, whose intensities are comparable to the transverse spin waves. This is a unique feature of $PrNi_2Si_2$, related to the large amplitude of the modulation of the ordered moment. It is in contrast to the pressure-induced AM phase in Pr metal, where the small amplitude modulation of the moments leads to barely visible amplitude modes.[24] The intensity of the phason mode decreases strongly with distance from the principal magnetic Bragg peak [see Figs. 5(c) and 5(f)], but is still observable in the neighborhood of the magnetic Bragg peak of the third harmonic at (1,1,0.61).

Individual scans along the $[0,0,\ell]$ and $[h,h,0]$ directions measured with $k_f = 1.5$ Å^{-1} are compared to the RPA results in Figs. 6, 7, and 8. They show, along with the comparison in Fig. 5, that the RPA theory gives a reasonable description of the major part of the inelastic scattering experiments concerning both excitation energies and relative intensities. However, a closer inspection of Figs. 6, 7, and 8 shows that there are two peaks in the energy range below 2 meV, where only one due to the phason mode is expected according to the RPA calculations.

In order to resolve the dispersion of the excitations at low energies more clearly, below 1.5 meV, we performed complementary scans with better resolution using $k_f = 1.3$ Å^{-1} as shown in Figs. 5(c) and 9(a). The two Q scans at $E = 0.7$ meV presented in Fig. 9 are just at the threshold for showing as separate peaks the two phason branches starting out from each magnetic zone center at (1,1,0.87) and (1,1,1.13). A series of fine resolution Q scans was made along $(1,1,L)$, and the phason branches become clearly distinguishable as separate peaks at the slightly higher energy $E = 0.8$ meV.

The temperature dependence of the scattering at (1,1,0.76) is shown in Fig. 10. The extra peak at about 1 meV in the longitudinal scattering range persists all the way up to T_N with a relative intensity that is essentially unchanged compared to low temperatures, which indicates that this low-energy mode is still there to interact with the longitudinal magnetic excitations also in the paramagnetic phase. The scan at T_N shows a broadening of the phason mode not captured by the RPA predictions, which may be due to critical fluctuations.

V. DISCUSSION

The magnetic ground state properties in $PrNi_2Si_2$ calculated within the MF approximation using the model in Table I agrees extremely well with the observations. The calculated (experimental) values for the Néel temperature are $T_N = 22.8$ (20) K and the low-temperature harmonics of the ordered moment are $M_1 = 2.49$ (2.35) μ_B and $M_3 = 0.45$ (0.4) μ_B.[27] Since the RKKY exchange interaction is long range and linewidth effects are unimportant at low temperatures, we expect the RPA to be an adequate approximation in the present case.[21] Indeed, both the energies and the intensities of the magnetic excitations in the longitudinally amplitude modulated phase

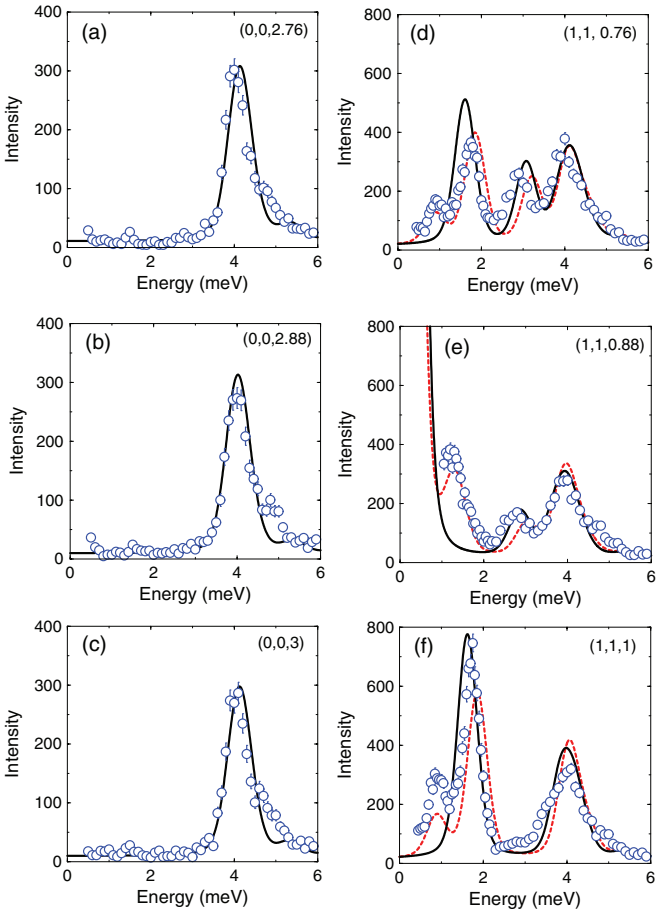

FIG. 6. (Color online) Energy scans for constant **Q** in the $[0,0,\ell]$ direction in $PrNi_2Si_2$ at $T = 1.6$ K using $k_f = 1.5$ Å^{-1}. (a)–(c) $\mathbf{Q} = (0,0,L)$, where only transverse spin waves are visible. (d)–(f) $\mathbf{Q} = (1,1,L)$, where longitudinal excitations and transverse spin waves are weighted about equally. The open (blue) circles are the experimental results and the (black) solid lines are the results predicted by the model in Table I. The dashed (red) lines in (d)–(f) are the scattering intensities derived from Eq. (B1) in the presence of an interaction between the phason and a local excitation.

in $PrNi_2Si_2$ below T_N are remarkably well described by the RPA theory using the same exchange parameters as determined previously for the paramagnetic phase.[25] This is illustrated in the overviews of Fig. 5 as well as by the black solid lines in the scans shown in Figs. 6–10. However, there is one important

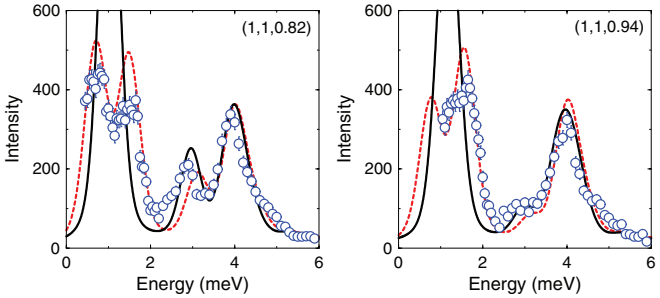

FIG. 7. (Color online) Additional energy scans for constant **Q** at $(1,1,L)$ in $PrNi_2Si_2$ at $T = 1.6$ K using $k_f = 1.5$ Å^{-1}. The symbols and lines are defined as in Fig. 6.

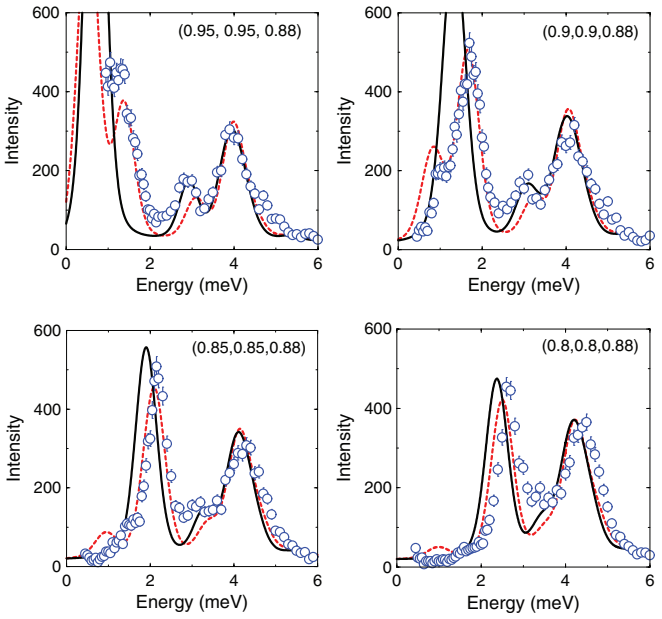

FIG. 8. (Color online) Energy scans for constant **Q** at $(H,H,0.88)$ when H is close to 1 in $PrNi_2Si_2$ at $T = 1.6$ K using $k_f = 1.5$ Å^{-1}. The symbols and lines are defined as in Fig. 6.

discrepancy: the experimental data indicate the presence of two peaks for energies below 2 meV, where the RPA model only predicts a single phason mode. This is seen both from data taken with $k_f = 1.5$ Å^{-1} (Figs. 6, 7, and 8) and from high-resolution data taken with $k_f = 1.3$ Å^{-1} [Fig. 5(c)].

What can be the reason for the extra peak? The CF model derived previously[16] is without doubt close to being the right one, as it provides a good description of the magnetization, the paramagnetic susceptibility, and the heat capacity, as well as reproducing the right positions and intensities of the paramagnetic CF levels observed in a polycrystalline sample.[25] This means that it can be excluded that the extra peak originates from one more single-site $J = 4$ MF level lying in the same energy range as the Γ_2 level (cf. Fig. 2). Forcing the exchange parameters in the RPA to give the principal amplitude mode at an energy of 1–2 meV (instead of at 3 meV) could solve the problem with the overall energy levels, but the intensities of

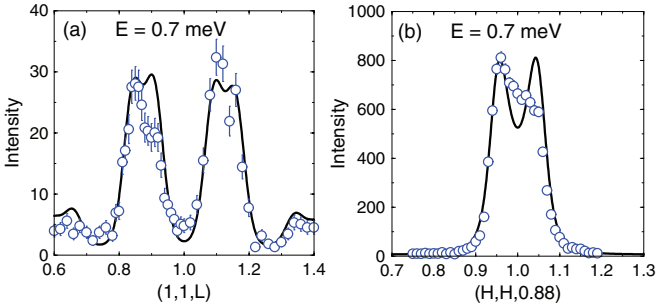

FIG. 9. (Color online) Q scans at $E = 0.7$ meV in $PrNi_2Si_2$ at $T = 1.6$ K: (a) along $(1,1,L)$ using $k_f = 1.3$ Å^{-1} and (b) along $(H,H,0.88)$ using $k_f = 1.5$ Å^{-1}. The symbols and lines are the same as in previous figures. Notice the two minor peaks in (a) due to the phasons in the neighborhood of the magnetic Bragg points of the third harmonic at $L = 0.61$ and 1.39.

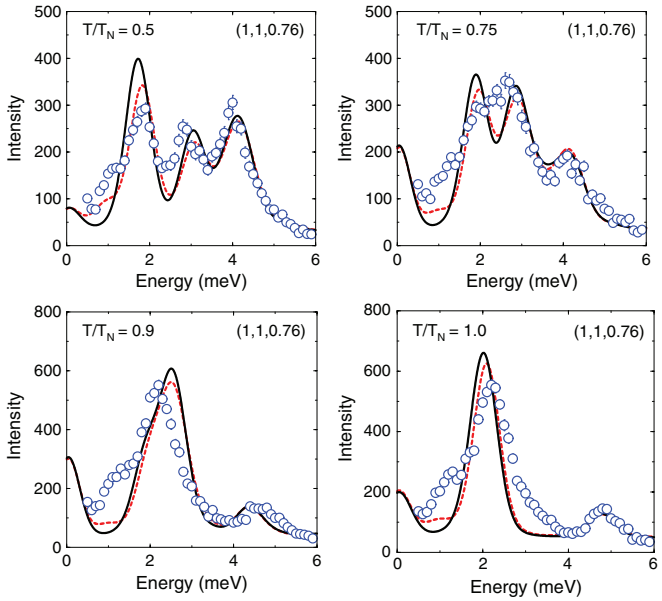

FIG. 10. (Color online) Temperature dependence of energy scans at $\mathbf{Q} = (1,1,0.76)$ in $PrNi_2Si_2$ using $k_f = 1.5$ Å^{-1}. The symbols and lines are the same as in previous figures. The corresponding scan at $T = 1.6$ K is shown in Fig. 6(d).

the modes would come out wrong. Experimentally, the upper one of the two modes dominates near the magnetic Brillouin zone boundaries [see Figs. 6(d) and 6(f)], whereas theoretically the amplitude mode will always have a lower intensity than the phason mode within the first magnetic Brillouin zone, since the amplitude mode is a derivative of the fundamental phason mode.

In order to try to solve the enigma with the two low-energy excitations, we have carried out a thorough analysis based on two alternative scenarios. In the first one, we investigated a coupling of the magnetic excitation to longitudinal phonons propagating along the c axis. As shown in Appendix A, our model does not account satisfactorily for the experimental observations. In the second scenario, we introduce an additional hypothetical dispersionless mode that hybridizes with the phason. This model, described in detail in Appendix B, provides a good description of the low-energy excitations in $PrNi_2Si_2$. However, this hypothetical mode cannot originate from a low-energy CF level and is also difficult to reconcile with the specific heat, which is well described by our MF theory.[15,16]

We finally briefly mention a few other possible explanations for the extra mode. (i) In view of the crystal quality and the stability of the $ThCr_2Si_2$ structure that $PrNi_2Si_2$ crystallizes into, it would be very unlikely that impurities or crystallographic imperfections would result in a dispersionless excitation that could hybridize with the phasons. (ii) While it is normally assumed that the electrons on the Ni ions or the conduction electrons only constitute a passive medium for establishing the RKKY interaction at the low energies in question (cf. the Pauli paramagnet YNi_2Si_2),[36] we cannot rule out the possibility that the extra mode could be related to an induced moment on the Ni ions. (iii) It is known that $CeNi_2Si_2$ is an intermediate-valence compound,[37,38] which may indicate that the $4f$ electrons of the Pr^{3+} ([Xe] $4f^2$) ions in the related, neighboring $PrNi_2Si_2$ compound are delocalized to some extent. This possibility has to be combined with that the study of the CF levels[15,16] did not detect any deviations from that expected for ions with two $4f$ electrons. (iv) The phonons might be able to create a bound state in combination with the Γ_2 excited level,[39] or the corresponding MF level in the ordered state, if there is a high spectral density of phonons with the right symmetry at energies in the range of 3–5 meV.

VI. CONCLUSION

The longitudinally amplitude-modulated magnetic phase of the induced-moment system $PrNi_2Si_2$ has been studied by inelastic neutron scattering at low temperatures, well below the Néel temperature. The characteristic longitudinally polarized excitations of this phase, a strongly dispersive gapless phason mode and several less dispersive amplitude modes at higher energies, coexist with nearly dispersionless transverse spin waves, whose energies are close to the amplitude modes. The amplitude modes are unusually strong, a fact related to the large amplitude modulation of the ordered moments, a quite unique feature of $PrNi_2Si_2$.

Both the energies and the intensities of all these modes are well accounted for in a random-phase approximation based on the crystal-field and exchange parameters determined from the paramagnetic properties of the system. The agreement between experiment and theory is surprisingly good in view of that no parameters have been adjusted. Minor modifications of the exchange couplings are expected to marginally improve the agreement.

The only major discrepancy between the calculations and the experiment is the presence of two excitations below 2 meV, where only one phason mode is expected theoretically. This observation cannot be accounted for in an RPA treatment of the Pr^{3+} $4f$ orbitals. We have investigated whether an extra excitation could originate from a hybridization between phasons and longitudinal acoustic phonons arising due to the modulation of the ordered moments. A better agreement is obtained by supposing that the phason hybridizes with a dispersionless mode at an energy of 1 meV. However, the physical origin of such a hypothetical excitation, which gives no magnetic contribution to the specific heat, remains mysterious. Further investigations should probably focus on the properties of the phonons and the band electrons in $PrNi_2Si_2$.

In conclusion, we have shown that $PrNi_2Si_2$ is an ideal system for studying the behavior of the magnetic excitations in an amplitude modulated magnetic structure, where the amplitude of the first harmonic of the ordered magnetic moment is large and the amplitude of the third harmonic is small. The system exhibits a rich dynamic spectrum with well-defined longitudinal excitations and transverse spin waves, which are well accounted for in an RPA model, except for the mysterious hybridization of the phason with an extra level of unknown origin.

ACKNOWLEDGMENTS

Fruitful discussions with Christoph Geibel are gratefully acknowledged. Financial support has been received from

Spanish MEC and FEDER Grants No. MAT2008-06542-C04-03 and No. MAT2011-27573-C04-02.

APPENDIX A: MAGNETOELASTIC EFFECTS

Here we investigate a scenario where the magnetic excitations couple to longitudinal phonons propagating along the c axis. This may be accounted for in terms of an effective ω-dependent quadrupole-quadrupole interaction.[21,23] The relevant magnetoelastic Hamiltonian based on the symmetry properties of the system is

$$\mathcal{H}_{\rm me}^{\rm dyn} = -\frac{1}{2}\sum_{ij}\mathcal{J}_{44}(ij,\omega)\mathcal{O}(i)\,\mathcal{O}(j), \tag{A1}$$

where $\mathcal{O}(i) \equiv O_2^0(i) + \alpha O_4^4(i)$ and the Fourier transform of the interaction for wave vectors along the c axis is given by

$$\mathcal{J}_{44}(\mathbf{q},\omega) = \mathcal{J}_{44}^0 \frac{1}{\pi^2}\frac{\omega_0^2\sin^2(\pi q)}{\omega_\ell^2(q)-\omega^2}, \quad \mathbf{q}\parallel\mathbf{c}^*, \tag{A2}$$

when assuming $q = |\mathbf{q}|$ somewhat smaller than 1.

The actual model has three parameters that are determined as follows. The dispersion of the longitudinal acoustic phonon mode along c is assumed linear $\omega_\ell(q) = \omega_0 q$, where the wave vector q is given in units of $2\pi/c$ and $\hbar\omega_0 = 10$ meV is taken assuming that the elastic properties of $PrNi_2Si_2$ and YNi_2Si_2 are similar.[16] The value of $\alpha = -0.153$ is chosen to minimize the magnetoelastic strain in the model. The estimated change of the lattice parameter c between zero temperature and 60 K is then 0.1%, in reasonable agreement with the experimental value of 0.07%.[40] The interaction strength along the c axis, $\mathcal{J}_{44}^0 = 1.8\times10^{-4}\times\pi^2$ meV, is obtained from a fit to the experimental excitation spectra along the c direction.

Considering only the magnetic part of the cross section, this magnetoelastic model accounts quite well for the scans near the magnetic Brillouin zone boundary along $(1,1,L)$. Close to the magnetic Bragg peak the magnetoelastic interaction may explain the observations only if the interaction is so anisotropic that it becomes negligible at wave vectors perpendicular to the c axis. This assumption is justified by the highly anisotropic crystal structure with c being more than twice as large as a and the absence of any anomaly in the temperature dependence of the lattice parameter a below 60 K.[40] The strong anisotropy would cause the phason mode energy to jump from about 0 to about 1.2 meV in the vicinity of the magnetic Bragg point when the wave vector is rotated from being parallel to being perpendicular to the c axis. This is in contradiction with our neutron scattering results obtained along $(H,H,0.88)$. Assuming, on the other hand, that the magnetoelastic interaction is isotropic would remove some of the discrepancies along the $(H,H,0.88)$ direction, but would not predict any extra inelastic peak near the zone center. While these shortcomings cannot rule out the importance of other magnetoelastic effects on the excitations in $PrNi_2Si_2$, it is clear that our experimental observations cannot derive from a simple hybridization of the phasons with a phonon mode.

APPENDIX B: INTERACTION WITH AN EXTRA MODE

Here we study a scenario where an additional hypothetical flat mode hybridizes with the phason mode. Evidence for such a hybridization is seen in, e.g., Fig. 5(c), which is redrawn in Fig. 11 on a blown up scale with focus on the region near the magnetic Bragg peak. This figure suggests that the phason mode, whose dispersion predicted by the RPA model is shown as a black solid line, is split into two branches by a hybridization with another mode lying at a constant energy of about 1 meV. In order to substantiate this hypothesis, we introduce an extra dispersionless level in a purely phenomenological way by adding a single-site interaction to the Hamiltonian of the form

$$\Delta\mathcal{H} = \sum_i [A J_z(i)\hat{K}_z(i) + \hat{K}(i)], \tag{B1}$$

where the dynamic variables $\hat{K}$ and $\hat{K}_z$ for the ith site act within their own two-dimensional vector space $|0\}$ and $|1\}$, obeying the rules

$$\hat{K}_z|0\} = |1\}, \quad \hat{K}_z|1\} = |0\}, \quad \hat{K}|0\} = 0, \quad \hat{K}|1\} = K_0|1\}. \tag{B2}$$

If $A = 0$, the extra excited level at the energy K_0 would show no dispersion and would not scatter neutrons. When A is nonzero, the K excitation is going to interact with the longitudinal J_z excitations and would gain dispersion and a nonzero neutron cross section via its mixing with the magnetic excitations.

The effects of this interaction, using $K_0 = 1.0$ meV and $A = 0.07$ meV, are shown by the red dashed lines in Fig. 11 and also by the red dashed lines in Figs. 6, 7, 8, and 10. The predictions of this simple model agree accurately with the experimental results obtained along $(1,1,L)$ at $T = 1.6$ K,

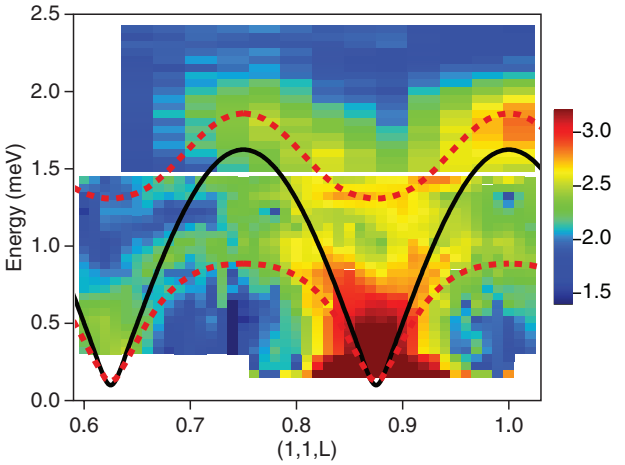

FIG. 11. (Color online) Neutron scattering intensity of the magnetic excitations in $PrNi_2Si_2$ at $T = 1.6$ K on a logarithmic scale as a function of wave vector and energy along $(1,1,L)$ using $k_f = 1.30$ Å^{-1} and flat analyzer. The data are the same as in Fig. 5(c), but focuses on the region near the magnetic zone center with a more sensitive intensity scale. The solid (black) line shows the phason dispersion as calculated using the RPA model. The (red) dashed lines are the dispersion of the phason after hybridization with a local excitation at 1 meV according to the model presented in Eq. (B1).

both concerning the dispersion (Fig. 11) and the intensities [Figs. 6(d)–6(f) and 7]. Along $(H,H,0.88)$ in Fig. 8, the weak intensity mode shows more dispersion than that expected from a local mode. With increasing temperature, the intensity of the extra excitation decreases more rapidly than observed in the experiment; cf. Figs. 6(d) and 10.

*Present address: European Spallation Source ESS AB, P.P. Box 176, SE-22100 Lund, Sweden.

[1] I. Urcelay-Olabarria, J. M. Perez-Mato, J. L. Ribeiro, J. L. García-Muñoz, E. Ressouche, V. Skumryev, and A. A. Mukhin, Phys. Rev. B **87**, 014419 (2013).
[2] T. Janssen, G. Chapuis, and M. D. Boissieu, *Aperiodic Crystals: From Modulated Phase to Quasicrystals* (Oxford University Press, Oxford, 2007).
[3] H. Z. Cummis, Phys. Rep. **185**, 211 (1990).
[4] R. Currat, in *Multicritical Phenomena*, edited by R. Pynn and A. T. Skjeltorp (Plenum, New York, 1983), p. 285.
[5] P. Bak, Rep. Prog. Phys. **45**, 587 (1982).
[6] C. Lacroix, J. Phys. Soc. Jpn. **79**, 011008 (2010).
[7] M. Kohno, O. A. Starykh, and L. Balents, Nature Phys. **3**, 790 (2007).
[8] E. A. Goremychkin, R. Osborn, B. D. Macaluso, D. T. Adroja, and M. Koza, Nature Phys. **4**, 766 (2008).
[9] T. Chattopadhyay, Science **264**, 226 (1994).
[10] A. P. Ramirez, Annu. Rev. Mater. Sci. **24**, 453 (1994).
[11] A. P. Ramirez, Nature (London) **421**, 483 (2003).
[12] Y. A. Izyumov, Physica B: Condens. Matter **174**, 9 (1991).
[13] A. Szytula and L. Leciejewicz, in *Handbook on the Physics and Chemistry of Rare Earths*, edited by K. A. Gschneidner, Jr. and L. Eyring (Elsevier Science, Amsterdam, 1989), Chap. 83.
[14] O. Moze, in *Handbook of Magnetic Materials*, edited by K. H. J. Buschow (Elsevier, Amsterdam, 1998), Chap. 4, p. 493.
[15] J. A. Blanco, D. Gignoux, and D. Schmitt, Phys. Rev. B **45**, 2529 (1992).
[16] J. A. Blanco, D. Schmitt, and J. C. Gómez-Sal, J. Magn. Magn. Mater. **116**, 128 (1992).
[17] J. Rossat-Mignod, in *Methods in Experimental Physics*, edited by K. Sköld and D. L. Price (Academic Press, Amsterdam, 1987), Vol. 23 C, p. 131.
[18] O. Stockert, J. Arndt, E. Faulhaber, C. Geibel, H. S. Jeevan, S. Kirchner, M. Loewenhaupt, K. Schmalzl, W. Schmidt, O. Si, and F. Steglich, Nature Phys. **7**, 119 (2011).
[19] D. K. Pratt, M. G. Kim, A. Kreyssig, Y. B. Lee, G. S. Tucker, A. Thaler, W. Tian, J. L. Zarestky, S. L. Bud'ko, P. C. Canfield, B. N. Harmon, A. I. Goldman, and R. J. McQueeney, Phys. Rev. Lett. **106**, 257001 (2011).
[20] W. C. Koehler, in *Magnetic Properties of Rare Earth*, edited by R. J. Elliot (Plenum, New York, 1972).
[21] J. Jensen and A. R. Mackintosh, *Rare Earth Magnetism: Structures and Excitations* (Oxford University Press, Oxford, 1991).
[22] R. M. Nicklow and N. Wakabayashi, Phys. Rev. B **51**, 12425 (1995).
[23] K. A. McEwen, U. Steigenberger, and J. Jensen, Phys. Rev. B **43**, 3298 (1991).
[24] J. Jensen, K. A. McEwen, and W. G. Stirling, Phys. Rev. B **35**, 3327 (1987).
[25] J. A. Blanco, R. M. Nicklow, and D. Schmitt, Phys. Rev. B **56**, 11666 (1997).
[26] H. Righi, D. Rached, S. Benalia, R. Khenata, S. Bin Omran, and A. H. Reshak, Comput. Mater. Sci. **54**, 303 (2012).
[27] J. A. Blanco, B. Fåk, E. Ressouche, B. Grenier, M. Rotter, D. Schmitt, J. A. Rodríguez-Velamazán, J. A. Campo, and P. Lejay, Phys. Rev. B **82**, 054414 (2010).
[28] R. Welter, G. Venturini, and B. Malaman, J. Alloys Compd. **329**, 69 (2001).
[29] J. A. Blanco, B. Fåk, R. M. Nicklow, B. Roessli, and D. Schmitt, Physica B **234–236**, 756 (1997).
[30] J. A. Blanco, R. M. Nicklow, and D. Schmitt, Physica B **213–214**, 327 (1995).
[31] M. Rotter, B. Fåk, and J. A. Blanco, J. Phys. Conf. Ser. **225**, 012008 (2011).
[32] A. M. Mulders, A. Yaouanc, P. Dalmas de Réotier, P. C. M. Gubbens, A. A. Moolenaar, B. Fåk, E. Ressouche, K. Prokeš, A. A. Menovsky, and K. H. J. Buschow, Phys. Rev. B **56**, 8752 (1997).
[33] J. H. van Vleck, *The Theory of Electric and Magnetic Susceptibilities* (Oxford University Press, London, 1932), Chap. 9.
[34] M. T. Hutchings, Solid State Phys. **16**, 227 (1964).
[35] M. Rotter, M. D. Le, A. T. Boothroyd, and J. A. Blanco, J. Phys.: Condens. Matter **24**, 213201 (2012).
[36] E. V. Sampathkumaran and I. Das, Phys. Rev. B **51**, 8178 (1995).
[37] M. Koterlyn, I. Shcherba, R. Yasnitskii, and G. Koterlyn, J. Alloys Compd. **442**, 176 (2007).
[38] J. J. Lu, M. K. Lee, Y. M. Lu, J. F. Chou, and L. Y. Jang, Solid State Commun. **135**, 505 (2005).
[39] P. Thalmeier and P. Fulde, Phys. Rev. Lett. **49**, 1588 (1982).
[40] E. V. Sampathkumaran, I. Das, A. Hayashi, and Y. Ueda, Solid State Commun. **93**, 123 (1993).